Influence of redox conditions on the intensity of Mars crustal magnetic anomalies

Stefanie BRACHFELD[1*], Deepa SHAH[1], Emily FIRST[2], Julia HAMMER[2], and Julie BOWLES[3]

[1]Department of Earth and Environmental Studies, Montclair State University, Montclair, New Jersey 07043, USA
[2]Department of Geology and Geophysics, University of Hawai'i, Honolulu, Hawai'i 96822, USA
[3]Department of Geosciences, University of Wisconsin-Milwaukee, Milwaukee, Wisconsin 53201, USA
[*]Corresponding author. E-mail: brachfelds@mail.montclair.edu

Abstract–We evaluate the relationship between the intensity of remanent magnetization and fO_2 in natural and synthetic Mars meteorites. The olivine-phyric shergottite meteorite Yamato 980459 (Y-980459) and a sulfur-free synthetic analog (Y-98*) of identical major element composition were analyzed to explore the rock magnetic and remanence properties of a basalt crystallized from a primitive melt, and to explore the role of magmatic and alteration environment fO_2 on Mars crustal anomalies. The reducing conditions under which Y-980459 is estimated to have formed (QFM-2.5; Shearer et al. 2006) were replicated during the synthesis of Y-98*. Y-980459 contains pyrrhotite and chromite. Chromite is the only magnetic phase in Y-98*. The remanence-carrying capacity of Y-980459 is comparable to other shergottites that formed in the fO_2 range of QFM-3 to QFM-1. The remanence-carrying capacity of these low fO_2 basalts is 1–2 orders of magnitude too weak to account for the intense crustal anomalies observed in Mars's southern cratered highlands. Moderately oxidizing conditions of >QFM-1, which are more commonly observed in nakhlites and Noachian breccias, are key to generating either a primary igneous assemblage or secondary alteration assemblage capable of acquiring an intense remanent magnetization, regardless of the basalt character or thermal history. This suggests that if igneous rocks are responsible for the intensely magnetized crust, these oxidizing conditions must have existed in the magmatic plumbing systems of early Mars or must have existed in the crust during secondary processes that led to acquisition of a chemical remanent magnetization.

INTRODUCTION

Intense crustal magnetic anomalies mapped in the southern cratered highlands during the Mars Global Surveyor mission have motivated investigations into the nature of the magnetic recording process and magnetic recording assemblage on Mars. Analysis of meteorites that originated on Mars and fell to Earth allows direct investigation of the composition of the Martian crust. There are presently 148 meteorites out of more than 60,000 collected on Earth that have been classified as having a Martian origin (Meteoritical Society Meteoritical Bulletin Database, http://www.lpi.usra.edu/meteor/metbull.php). The majority of these are the igneous Shergotty–Nakhla–Chassigny (SNC) meteorites. The young crystallization of SNC meteorites and their bulk compositional differences

with orbiter and rover measurements of Mars surface materials (Nyquist et al. 2001; Boynton et al. 2007; McSween et al. 2009; Agee et al. 2013; Humayun et al. 2013) make them unlikely candidate lithologies for the Noachian crust that carries the intense magnetic anomalies. Although their provenance on Mars is unknown, SNC meteorites are direct samples of Mars and are indisputably igneous in origin. Therefore, SNC meteorites are attractive targets for laboratory experimental studies concerning the magmatic contribution to Martian crust and the ability of primitive rocks (those derived directly from the Mars mantle and experiencing little modification during ascent and emplacement at the surface) to acquire a thermoremanent magnetization. These processes are relevant to confirming or refuting an igneous origin for the intense crustal magnetic anomalies in the southern

cratered highlands (Acuña et al. 1999, 2001; Connerney et al. 1999).

Multicomponent silicate melts with compositions matching those of the inferred meteorite parent liquids can be synthesized to examine the consequences of various environmental parameters on mineralogy, texture, and physical properties (Johnson et al. 1991; McSween et al. 1996; McCoy and Lofgren 1999). Moreover, SNC meteorites preserve information about the composition of the Mars mantle as well as the intrinsic conditions, notably redox state during magma generation in the Mars mantle and its subsequent emplacement in the crust and on the surface. Redox state is particularly important for magnetic remanence acquisition, as it controls the partitioning of Fe^{2+} and Fe^{3+} into silicates, sulfides, and oxides, which have a wide range of magnetic properties and remanence recording abilities. Published estimates of magmatic oxygen fugacity (fO_2) are available for 21 shergottites (the largest subset of the recognized Martian meteorites), which include olivine-phyric and basaltic to lherzolitic compositions. The magma source regions represented by these samples span oxidation states between at least 0.4 $\log_{10}$ units above the quartz–fayalite–magnetite (QFM) reference buffer and 5 $\log_{10}$ units below the QFM buffer (McSween et al. 1996; Ghosal et al. 1998; Herd et al. 2001, 2002; Herd 2003, 2006; Wadhwa 2001; Goodrich et al. 2003; McCanta et al. 2009; Lorand et al. 2005; Shearer et al. 2006; Hui et al. 2011). This is comparable to the fO_2 range of QFM-3.6 to QFM+0.5 determined from Spirit Mars Exploration Rover in situ measurements of unaltered basalts in Gusev Crater (Schmidt et al. 2013).

Previous work by our group (Brachfeld and Hammer 2006; Hammer 2006; Bowles et al. 2009) investigated the role of oxygen fugacity in controlling the mineralogy and magnetic properties of basalts with high Fe/Al (meteorite-type) and low Fe/Al (terrestrial-type) character. Notably, both compositions were based on a hypothetical liquid that is calculated to be in equilibrium with the phase assemblage of Chassigny (Johnson et al. 1991). This study leverages our previous work by adopting similar experimental and analytical methodologies, and (a) basing the synthetic starting material on a meteorite whole rock composition that is widely accepted to represent a partial melt of the Martian mantle (Musselwhite et al. 2006; Usui et al. 2008; Filiberto and Dasgupta 2011), (b) focusing experiments at the magmatic fO_2 indicated by the meteorite's mineral compositions (Shearer et al. 2006; Usui et al. 2008), and (c) coupling magnetic investigations with detailed petrologic characterization of the meteorite and synthetic basalts. We place our results within the larger context of Mars meteorite fO_2

and remanence-carrying ability, and demonstrate that moderately oxidizing conditions > QFM-1, whether magmatic or occurring during later alteration processes, are key to producing a magnetic mineral assemblage that is capable of carrying the Mars crustal anomalies.

SAMPLES AND METHODS

Yamato 980459 (hereafter Y-980459) was collected in Antarctica in 1998 near the Yamato Mountains and is curated at the National Institute of Polar Research of Japan. Y-980459 is an olivine-phyric shergottite (Greshake et al. 2004) with an Sm-Nd age of 472 $\pm$ 47 Ma (Shih et al. 2005). Y-980459 is described as an Mg-rich primitive rock that has undergone little fractionation and is therefore likely to be in equilibrium with a mantle assemblage (Musselwhite et al. 2006). Y-980459 formed at 1 $\log_{10}$ unit above the iron-wüstite (IW) buffer, which is equivalent to QFM-2.5 at the 1 atm liquidus temperature (Shearer et al. 2006). Y-980459 is an Fe-rich basalt and contains both Fe-Cr spinels and iron sulfides. A sulfur-free synthetic analog, named Y-98*, contains only Fe-Cr spinels. The samples are otherwise identical with respect to major element composition (Table 1).

Four chips of Y-980459 and a polished thin section were obtained from the Japan National Institute for Polar Research. The sulfur-free analog Y-98* was synthesized at the University of Hawai'i at Mānoa using oxide and carbonate reagents following methods described in Hammer (2006). Large beads of powdered starting material were held at 1385 °C in a reducing atmosphere of ~IW+1 for 12 h and subjected to a two-stage cooling history consisting of a 28 °C h^{-1} ramp to 1113 °C followed by a 320.6 °C h^{-1} ramp to 909 °C. Experiments were terminated by drop-quenching into water. Two dynamic crystallization runs of Y-98* (denoted Y-98* f48 and Y-98* f49) were performed to test the reproducibility of the synthesis process and run products. Three beads were generated in each run, with one bead retained for petrographic analysis at the University of Hawai'i and the other two utilized for magnetic studies at Montclair State University.

Petrographic imaging and electron microprobe analyses were conducted on a JEOL JXA-8500F Field Emission Hyperprobe at the University of Hawai'i at Mānoa, with an accelerating voltage of 20 kV and a beam current of 20 nA. Wavelength-dispersive spectrometry (WDS) single-spot analyses of Si, Ti, Al, Cr, Fe, Mn, Mg, Ni, and S were gathered for chromite and iron-nickel sulfides, with on-peak counting times of 20–60 s (Table 2). Calibration was based on chromite USNM 117075 (Al, Mg, Fe, Cr), Staunton meteorite troilite (S), sphene glass (Si, Ti), Verma garnet (Mn),

Table 1. Composition (wt%) of Y-980459 and Y-98*.

	Bulk experimental glass[a]	Greshake et al. (2004)[d]	Misawa (2004)[d,e]	Shirai and Ebihara (2004)[d,f]
SiO_2	49.84	49.4	48.70	49.9
TiO_2	0.58	0.48	0.54	0.532
Al_2O_3	5.92	6.0	5.27	5.17
Cr_2O_3	0.67	0.71	0.71	0.695
FeO	17.85[b]	15.8	17.53	17.3
MnO	0.47	0.43	0.52	0.481
MgO	18.34	18.1	19.64	18.7
NiO	n.a.[c]	0.03	0.034	0.0258
CaO	6.69	7.2	6.37	6.83
Na_2O	0.14	0.80	0.48	0.651
K_2O	0.01	0.02	<0.02	0.0156
P_2O_5	n.d.	0.31	0.29	n.a.
S	n.a.	0.07	0.09	0.1650
Total%	100.51	99.35	100.17	100.47

[a]Synthetic Y-98* composition determined from the average of five electron microprobe analyses of a glass bead (sample ID f46i). Low concentrations of alkali oxides and P_2O_5 (n.d. = not detected) are attributed to volatilization during fusion.

[b]Y-98* FeO value is an interpolation based on an FePt wire composition of 20% Fe, preannealing.

[c]Ni is present in Y-98*, but was not analyzed (n.a.) as analytical conditions used for major elements precluded accurate Ni determination.

[d]Published Y-980459 composition.

[e]Original wt% Ni and wt% FeS have been converted to wt% NiO and wt% S, with appropriate adjustment to wt% FeO.

[f]Original ppm Ni and ppm S have been converted to wt% NiO and wt% S.

and NiO (Ni) standards. Linear background fits were used, along with the Phi-Rho-Z matrix corrections of Armstrong/Love Scott (Armstrong 1988). Images were also obtained with the JEOL 5900 LV scanning electron microscope.

Magnetic analyses were conducted at Montclair State University, New Jersey. Magnetic susceptibility (χ) was measured on an AGICO KLY-4 Kappabridge. Natural remanent magnetization (NRM), anhysteretic remanent magnetization (ARM), and isothermal remanent magnetization (IRM) were measured on an AGICO JR-6 Spinner Magnetometer, and subjected to alternating field (AF) demagnetization on a D-tech D-2000 AF Demagnetizer. ARM was imparted using a DC field of 0.05 mT and a peak alternating field of 100 mT. A 1 T isothermal remanent magnetization (IRM) was imparted using an ASC Scientific Impulse Magnetizer. The hysteresis parameters saturation magnetization, saturation remanence, coercivity, coercivity of remanence, and high-field magnetic susceptibility (M_S, M_{RS}, B_C, B_{CR}, and χ_{hf}, respectively) were measured on a Princeton Measurements Corp. Vibrating Sample Magnetometer (VSM) in a 1 T peak

field. Susceptibility versus temperature curves (20–400 °C) were measured on an AGICO KLY4 Kappabridge in an argon atmosphere. Low-temperature magnetic behavior was measured on a Quantum Design Magnetic Properties Measurement System (MPMS) at the Institute for Rock Magnetism (IRM), University of Minnesota. An isothermal remanent magnetization ($M_{R(20K)}$) was imparted at 20 K in a 2.5 T field after cooling from 300 K in the presence of a 2.5 T field (FC = field cooled), and again at 20 K in a 2.5 T field after cooling from 300 K in zero applied field (ZFC = zero-field cooled). A room temperature saturation isothermal remanent magnetization was imparted in a 2.5 T field at 300 K (denoted $M_{R(300K)}$) and monitored during cooling to 20 K and warming back to 300 K. Magnetic susceptibility versus temperature was measured between 20 and 300 K as a function of applied field frequency between 1 and 1000 Hz.

RESULTS

Petrographic and Compositional Analyses

Y-980459 contains olivine and pyroxene phenocrysts encased in a glassy groundmass of Fe-rich olivine, chromite, dendritic olivine, chain-like augite, and iron sulfide droplets (e.g., Greshake et al. 2004; Shearer et al. 2006; Usui et al. 2008) (Fig. 1a). Y-980459 is noteworthy in that it lacks plagioclase and its shock-metamorphosed product maskelynite. Previous studies of Y-980459 list chromite as the only spinel group mineral present, with chromite abundance estimated at 0.5%, and iron sulfide abundance at 0.3% (Greshake et al. 2004; Usui et al. 2008). Similarly, chromite is the only oxide observed in this study. With the exception of sulfides, the bulk mineralogy of synthetic Y-98* closely matches the meteorite. Y-98* contains pyroxene, euhedral olivine, and Fe-Cr spinels 10 μm in diameter. Nearly all Y-98* samples lack plagioclase, with the exception of one bead that contains minor amounts (Fig. 2).

Y-980459 Fe-Cr spinels analyzed in this study have an average composition of $Cr_{1.54}Fe_{0.67}Mg_{0.40}Al_{0.32}Ti_{0.04}O_4$. Some of the Fe-Cr spinels contain slightly more Ti and slightly less Cr (Fig. 3; Table 2). The compositions of the Fe-Cr spinels in synthetic Y-98* are very similar to those in the meteorite (Table 2), with an average composition of $Cr_{1.60}Fe_{0.61}Mg_{0.46}Al_{0.28}Ti_{0.02}Mn_{0.01}O_4$. All spinel analyses in both the meteorite and the synthetic basalt plot close to chromite composition in the Cr-(Al + Ti)-(Fe + Mg) ternary system (Fig. 3b). None of the grains analyzed via EMPA resemble titanomagnetite (Fig. 3b).

Table 2. Sulfide (wt%) and Cr spinel (wt% oxide) compositions.

Sample ID	Si	Ti	Al	Cr	Fe	Mn	Mg	Ni	S	Total
Y-980459 Sulfides with totals >98%										
Sulfide 1	0.13	0.00	0.03	0.03	53.01	0.00	0.00	6.94	37.94	98.08
Sulfide 3	0.47	0.02	0.17	0.00	59.85	0.02	0.00	1.14	36.58	98.24
Sulfide 7	0.41	0.02	0.21	0.67	58.05	0.03	0.00	1.26	38.23	98.88
Sulfide 11	0.36	0.02	0.14	0.28	56.37	0.01	0.00	4.02	37.34	98.54
Sulfide 12	0.42	0.02	0.12	0.02	57.90	0.00	0.00	1.45	38.71	98.64
Sulfide 14	0.43	0.02	0.16	0.00	59.68	0.00	0.00	0.84	37.21	98.35
Sulfide 16	0.42	0.01	0.15	0.00	58.41	0.01	0.00	0.61	38.71	98.32
Average	**0.38**	**0.01**	**0.14**	**0.14**	**57.61**	**0.01**	**0.00**	**2.32**	**37.82**	**98.44**
Y-980459 Cr Spinels with totals >98%										
Chromite 2	0.65	0.20	8.05	59.13	22.40	0.39	7.79	0.02	0.00	98.64
Chromite 3	0.12	6.41	10.92	44.53	26.93	0.43	8.89	0.02	0.01	98.25
Chromite 6	0.69	0.41	5.77	60.98	22.45	0.42	7.34	0.03	0.01	98.10
Chromite 8	0.92	0.91	10.21	53.14	24.45	0.42	8.18	0.02	0.04	98.27
Chromite 9	0.83	0.49	5.94	60.74	22.59	0.39	7.34	0.03	0.01	98.34
Chromite 14	0.66	0.18	6.36	61.44	22.01	0.41	7.76	0.01	0.00	98.83
Average	**0.64**	**1.43**	**7.87**	**56.66**	**23.47**	**0.41**	**7.88**	**0.02**	**0.01**	**98.40**
Y-98* f48iii Cr Spinels with totals >98%										
Y98-f48iii_spinel 1a	0.83	0.64	6.93	59.24	21.54	0.38	8.49	0.00	n.a.	98.05
Y98-f48iii_spinel 1b	0.81	0.68	7.11	60.14	19.86	0.34	9.78	0.00	n.a.	98.72
Y98-f48iii_spinel 3	0.94	0.67	7.01	59.72	20.40	0.38	9.96	0.00	n.a.	99.07
Y98-f48iii_spinel 4	0.97	0.58	6.73	59.18	21.51	0.36	9.20	0.00	n.a.	98.54
Y98-f48iii_spinel 5	0.90	0.65	6.79	59.69	21.18	0.36	9.25	0.00	n.a.	98.83
Y98-f48iii_spinel 8	0.63	0.84	7.24	59.75	19.55	0.34	9.92	0.01	n.a.	98.26
Average	**0.84**	**0.68**	**6.97**	**59.62**	**20.67**	**0.36**	**9.43**	**0.00**	**n.a.**	**98.58**
Y-98* f49ii Cr Spinels with totals >98%										
Y98-f49ii_spinel 1	0.68	0.72	7.04	60.73	20.16	0.32	9.51	0.01	n.a.	99.17
Y98-f49ii_spinel 1 rim	0.93	0.88	7.33	58.30	21.72	0.36	8.75	0.00	n.a.	98.26
Y98-f49ii_spinel 2a	0.80	0.80	7.34	59.47	20.71	0.34	9.25	0.00	n.a.	98.71
Y98-f49ii_spinel 3a	0.59	0.77	7.40	60.54	19.38	0.32	9.81	0.00	n.a.	98.82
Y98-f49ii_spinel 3b	0.76	0.75	6.97	59.43	22.48	0.37	7.54	0.01	n.a.	98.32
Y98-f49ii_spinel 4a	0.62	0.80	7.43	59.77	19.68	0.31	9.70	0.01	n.a.	98.30
Y98-f49ii_spinel 4b	0.90	0.90	7.44	58.54	22.02	0.35	8.16	0.00	n.a.	98.30
Y98-f49ii_spinel 5	0.78	0.69	6.57	60.61	20.25	0.33	9.34	0.00	n.a.	98.57
Y98-f49ii_spinel 7	0.96	0.80	7.24	58.10	22.62	0.41	8.60	0.00	n.a.	98.72
Y98-f49ii_spinel 8a	0.93	0.62	6.80	58.92	20.77	0.37	9.59	0.00	n.a.	98.00
Y98-f49ii_spinel 8b	0.85	0.53	6.51	60.55	19.79	0.36	10.33	0.00	n.a.	98.92
Y98-f49ii_spinel 9	0.98	0.61	6.29	59.98	21.56	0.36	8.89	0.00	n.a.	98.67
Y98-f49ii_spinel 10	0.83	0.80	6.90	59.72	21.00	0.33	8.70	0.00	n.a.	98.28
Average	**0.82**	**0.74**	**7.02**	**59.59**	**20.93**	**0.35**	**9.09**	**0.00**	**n.a.**	**98.54**

n.a. = not analyzed.

Previous studies have reported that iron sulfide droplets in Y-980459 range in size from 5 to 30 μm and occur within the glassy groundmass or very rarely as inclusions in olivine (Greshake et al. 2004). In this study, we similarly observed small sulfide droplets as well as rare grains up to 100 μm in diameter, with both types exhibiting fractures (Fig. 1). The iron sulfides contain 0.07 to 6.94 wt% Ni (Fig. 3; Table 2). The metal/sulfur ratio varies between 0.87 and 0.96, with an average value of 0.90 and an average composition of $Fe_{0.45}Ni_{0.02}S_{0.52}$, or $(Fe, Ni)_9S_{10}$.

Rock Magnetic Analyses

The four Y-980459 sample chips have χ values of 5.14 to 6.34*10^{-7} m^3 kg^{-1} (Table 3), comparable to other shergottites formed at reducing conditions (<QFM − 2) such as DaG 476, 489, 670, and 1037, Dho 19, SAU
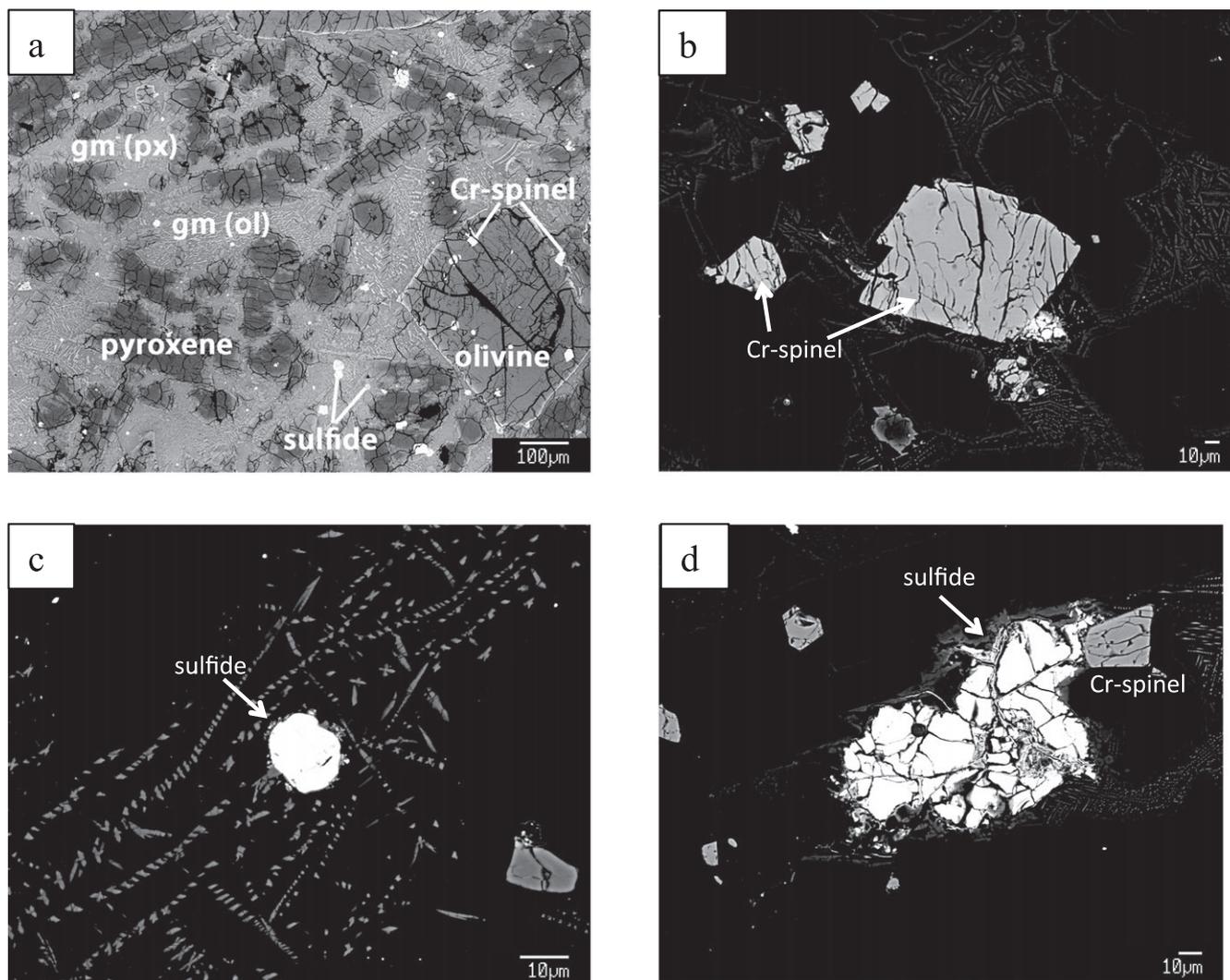
Fig. 1. Backscatter electron (BSE) images of Y-980459. a) Bulk mineralogy; ol = olivine, px = pyroxene, gm = groundmass. b) Fractured chromite grains surrounded by groundmass. c) 10 μm sulfide droplet surrounded by groundmass. d) A 100 μm fractured sulfide grain surrounded by groundmass.

005 and 0990, EET A79001A, Shergotty, and Zagami (Rochette et al. 2005). NRM values for Y-980459 range from 0.774 to $4.20*10^{-5}$ Am^2 kg^{-1}, similar to NRM values previously reported by Hoffman et al. (2010). ARM values for Y-980459 range from 17.5 to $22.0*10^{-5}$ Am^2 kg^{-1}. The χ, NRM, and ARM values for synthetic Y-98* are generally 0.5 to 1 order of magnitude weaker than the meteorite (Fig. 4; Table 3).

Y-980459 acquired a remanence during AF demagnetization of the NRM, with two samples displaying a nearly five-fold increase above the starting NRM value (Fig. 4a). This is likely a gyroscopic remanent magnetization (GRM), which is commonly observed in iron sulfides (Thompson 1990; Snowball 1997). Three of the four Y-980459 samples display normal AF demagnetization profiles for ARM and

IRM, in which the intensity of remanence decays steadily with peak applied field (Figs. 4b and 4d). The NRM (data not shown) and ARM AF demagnetization trends for synthetic Y-98* show no smooth decay with applied field (Fig. 4c). The intensity of IRM in Y-98* displays a steady decrease as a function of peak applied field during AF demagnetization (Fig. 4d), although its median destructive field (MDF, 20 mT for Y-98*) is lower than for Y-980459 (35 mT).

Y-980459 M_R/M_S values are near 0.3, and B_{cr} values are near 62 mT (Table 3). Hysteresis parameters M_S and M_R are 0.5 to 2 orders of magnitude weaker in Y-98* than in the meteorite. Y-98* plots in the lower-right corner of the pseudo-single domain (PSD) region of a Day plot (Day et al. 1977), along with other Cr-bearing Fe-rich basalts synthesized at IW through QFM
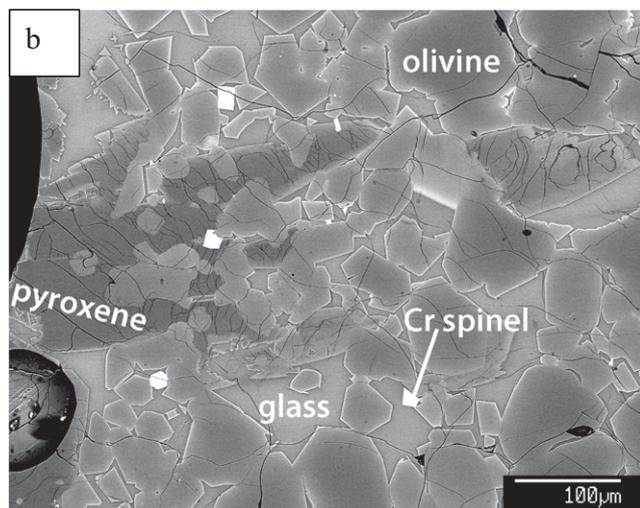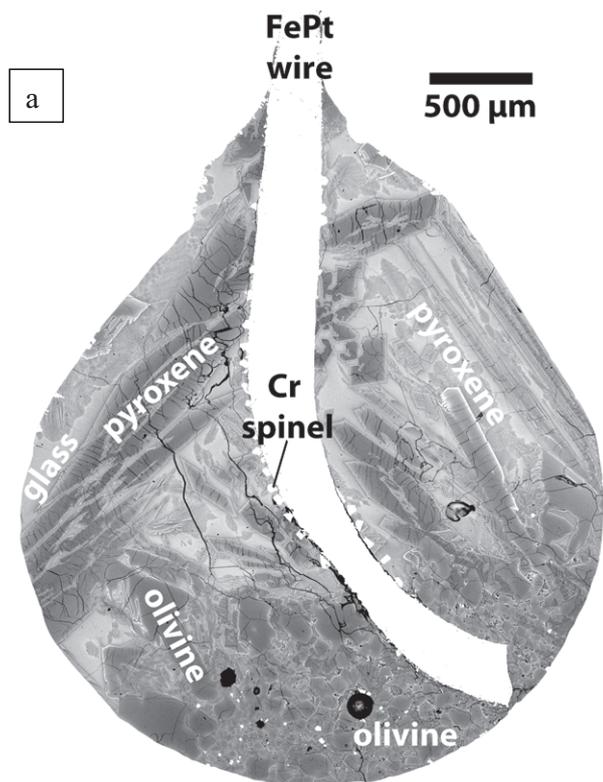
Fig. 2. a) BSE mosaic image of synthetic Y-98* f49ii. Molten beads are suspended from Fe-plated Pt wires during synthesis. The FePt wire in this image is oriented in the up–down direction, showing the orientation of the bead within the furnace. Concentration of olivine at the base of the bead suggests gravitational settling of crystals within the molten bead. The bead is broken into chips to remove the FePt wire prior to magnetic analysis. b) BSE close-up of synthetic Y-98* 48iii showing olivine, pyroxene, and Cr spinels.

Fig. 3. a) Fe-Ni-S ternary diagram with compositions of Y-980459 Fe-Ni sulfides (gray squares) for which totals are >98%. Troilite (open circle) and pyrrhotite (solid circle) are shown for comparison. b) Cr-(Al + Ti)-(Fe + Mg) ternary diagram with six Cr-Fe spinel analyses from Y-980459 and 24 analyses from synthetic Y-98* (analyses for which totals are >98%). Compositions are tightly clustered for both the natural and synthetic meteorite. Chromite ($FeCr_2O_4$) and $Fe_{2.4}Ti_{0.6}O_4$ (TM60) are shown for comparison.

conditions (Bowles et al. 2009). M_R/M_S values are between 0.10 and 0.20. B_{cr} values for Y-98* are high (43–97 mT) and S-ratios are below 0.70, suggesting that a high-coercivity mineral is present, one that is unresponsive to the low DC field used for ARM acquisition (50 µT) but that is magnetized by the 1 T pulse field used to impart IRM.

High-temperature (20–400 °C) thermomagnetic curves for Y-980459 (Fig. 5a) show a steady loss of susceptibility with increasing temperature up to 240 °C, a brief plateau in signal between 240 and 310 °C, and loss of susceptibility with increasing temperature resuming at 310 °C. There is no clear evidence of the lambda transition for hexagonal pyrrhotite (Fe_9S_{10}). Y-980459 samples do not exhibit the 34 K order–disorder transition associated with monoclinic pyrrhotite (Fe_7S_8) (Dekkers et al. 1989; Rochette et al. 1990). There is no abrupt loss in M_S (data not shown) or M_R at 34 K during warming (Fig. 5b), or are there noteworthy features in the

Table 3. Magnetic properties of natural and synthetic Y-980459.

| Sample ID	Mass (g)	χ_{lf} (m^3 kg^{-1})	χ_{hf} (m^3 kg^{-1})	NRM (Am^2 kg^{-1})	ARM (Am^2 kg^{-1})	IRM (Am^2 kg^{-1})	M_S (Am^2 kg^{-1})	M_R (Am^2 kg^{-1})	M_R/M_S	B_C (mT)	B_{CR} (mT)	B_{CR}/B_C	S-ratio
Natural Y-980459													
Chip 1	0.0886	6.22E-07	3.59E-07	4.20E-05	2.20E-04	1.41E-02	4.38E-02	1.37E-02	0.312	32.53	63.33	1.95	0.89
Chip 2	0.0847	5.14E-07	3.50E-07	1.19E-05	1.75E-04	1.35E-02	3.98E-02	1.29E-02	0.322	33.20	62.25	1.88	0.88
Chip 3	0.0351	6.34E-07	3.55E-07	3.54E-05	1.98E-04	1.42E-02	4.09E-02	1.26E-02	0.308	31.06	61.86	1.99	0.87
Chip 4	0.0910	5.33E-07	3.56E-07	7.74E-06	1.83E-04	1.41E-02	4.12E-02	1.33E-02	0.321	32.62	62.26	1.91	0.87
Average	–	5.76E-07	3.55E-07	2.43E-05	1.94E-04	1.40E-02	4.14E-02	1.31E-02	0.316	32.35	62.43	1.93	0.88
Synthetic Y98*													
Y98-f48i	0.0598	3.80E-07	3.48E-07	2.61E-05	2.44E-05	1.54E-03	5.88E-03	1.26E-03	0.214	24.58	97.66	3.97	0.52
Y98-48ii	0.1030	3.56E-07	3.25E-07	1.07E-05	1.11E-05	1.05E-03	4.64E-03	6.14E-04	0.132	14.68	78.16	5.32	0.60
Y98-f49i	0.0641	3.88E-07	2.85E-07	1.02E-05	2.03E-05	1.74E-03	7.04E-03	9.66E-04	0.137	12.59	43.14	3.43	0.78
Y98-f49iii	0.0790	3.91E-07	3.31E-07	2.24E-05	1.42E-05	5.84E-04	5.89E-03	5.82E-04	0.099	10.96	48.52	4.43	0.63
Average	–	3.79E-07	3.22E-07	1.74E-05	1.75E-05	1.23E-03	5.86E-03	8.55E-04	0.145	15.70	66.87	4.29	0.63
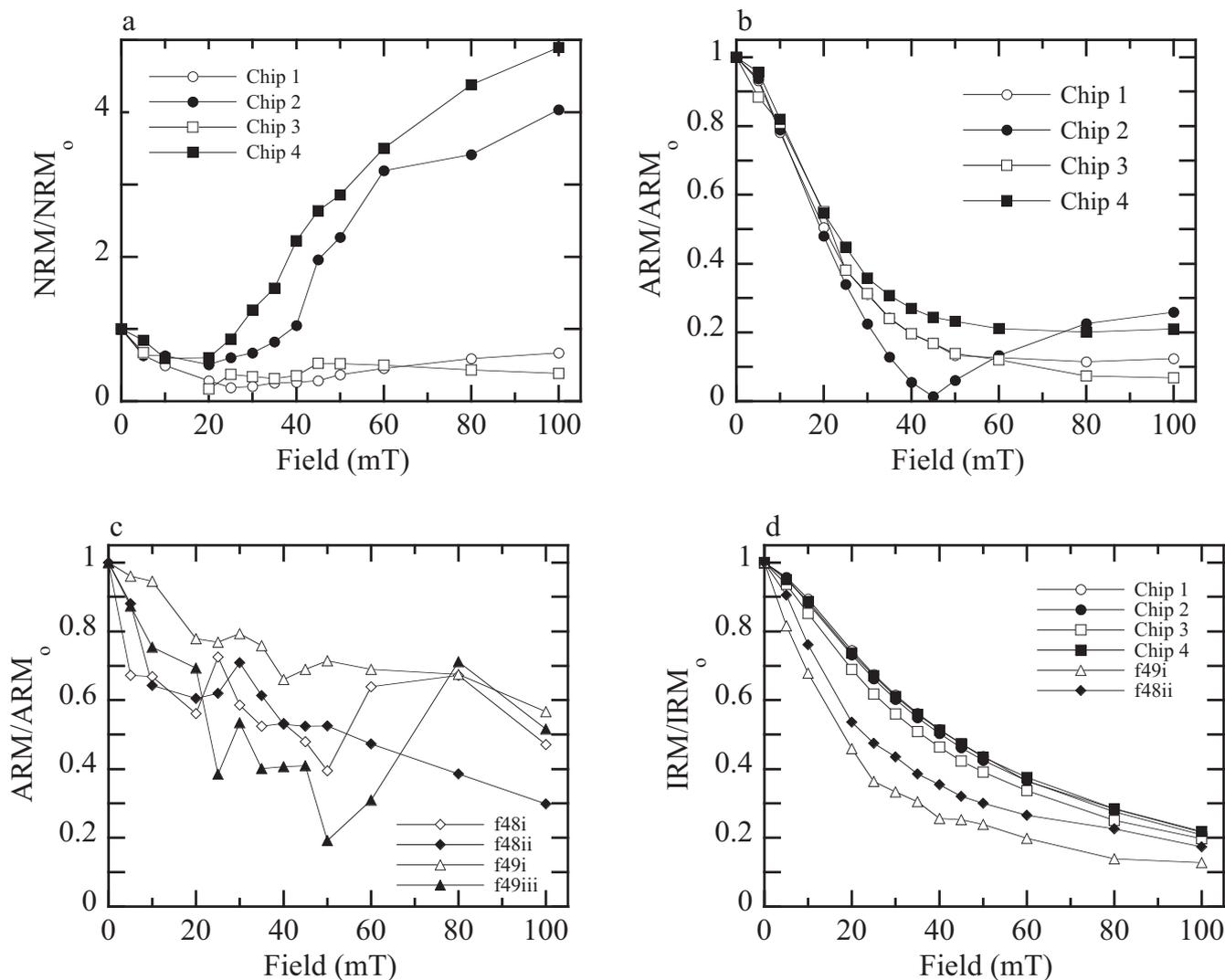
Fig. 4. a) Alternating field (AF) demagnetization of the NRM in Y-980459, which acquires a GRM during AF demagnetization. The differences in the four curves are likely due to heterogeneous pyrrhotite abundance in the four sample chips. b) AF demagnetization of ARM in Y-980459. Chip 2 acquires a GRM at the 50 mT demagnetization step. c) AF demagnetization of ARM in synthetic Y-98*. d) AF demagnetization of IRM in Y-980459 and the two more strongly magnetic samples of synthetic Y-98*.

room temperature $M_{R(300\ K)}$ cooling–warming curves (Fig. 5c). There are no indications of a 34 K feature in the first derivatives of the FC–ZFC curves, or in the low-temperature susceptibility curves (Fig. 5d), which display only paramagnetic behavior. There is no frequency dependence of susceptibility. However, the FC curve is higher than the ZFC curve below 170 K. There is an inflection point in the FC and ZFC M_R-T profiles (Fig. 5b) and a local maximum in the dM_R/dT profiles at 55–60 K (data not shown).

Fig. 5. a) χ versus temperature measured from 20 to 400 °C for Y-980459 chip 1. b) Y-980459 chip 4 temperature-dependent intensity of a 2.5 T saturation remanence magnetization imparted at 20 K ($M_{R(20K)}$) following cooling in a 2.5 T field (FC = field cooled) and again after cooling from 300 to 20 K in zero applied field (ZFC = zero-field cooling). c) Y-980459 chip 4 temperature-dependent intensity of a room temperature saturation isothermal remanent magnetization imparted in a 2.5 T field at 300 K ($M_{R(300K)}$), and monitored during one cycle of cooling and warming. d) In-phase component of χ versus temperature (20–300 K) and versus frequency of the applied field for Y-980459 chip 4. e) FC and ZFC $M_{R(20K)}$-T curves and f) $M_{R(300K)}$ curves for synthetic Y-98* f49iii. Shifts in the $M_{R(300K)}$ profile at 95 and 115 K are likely due to sample chips shifting inside the capsule during the measurements.
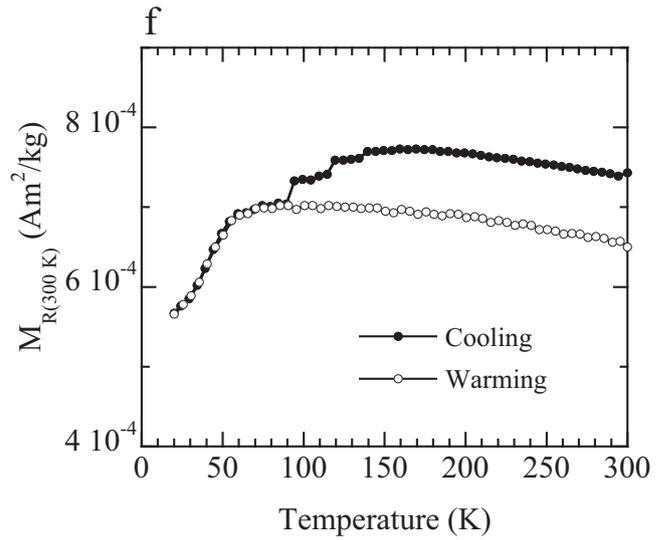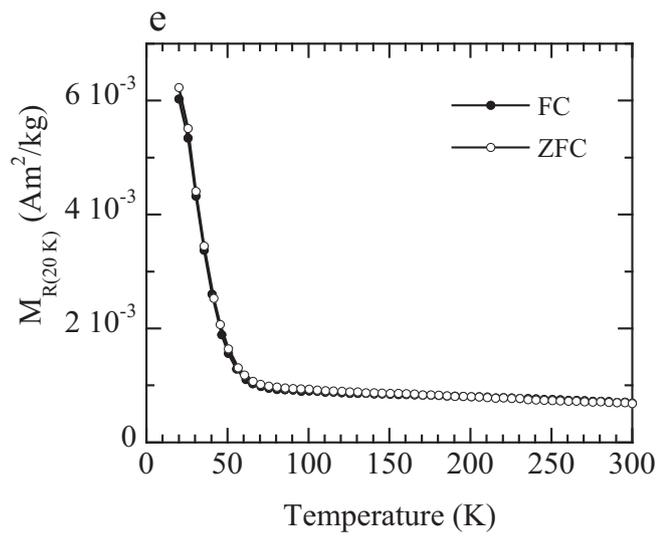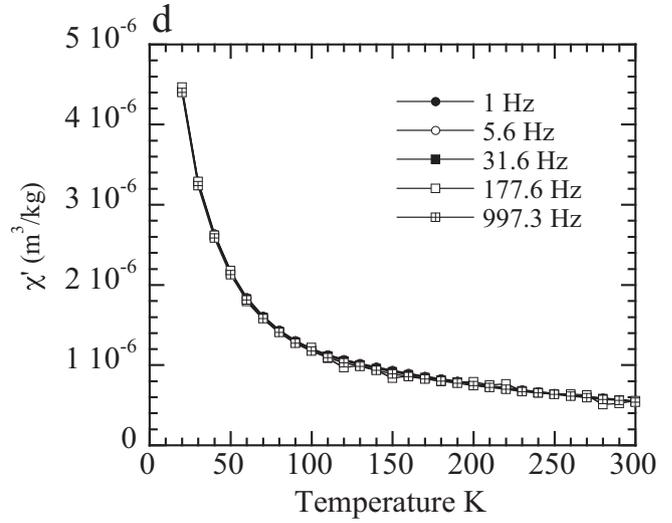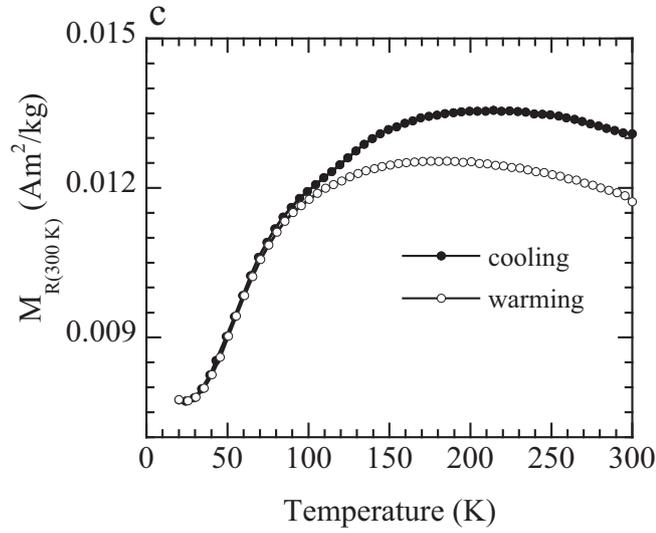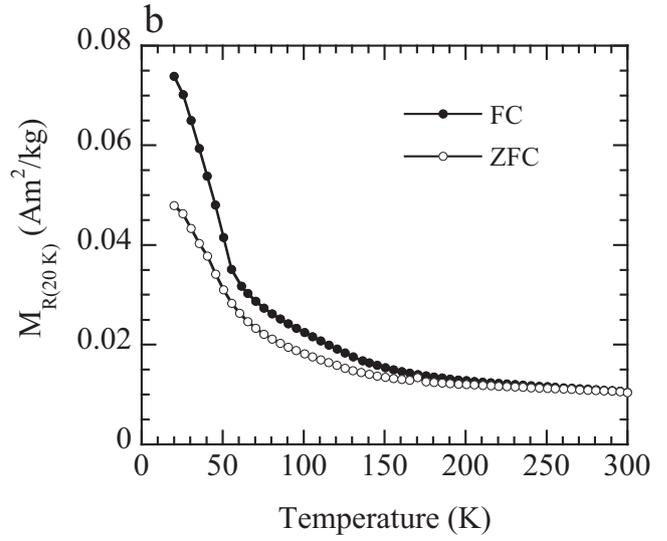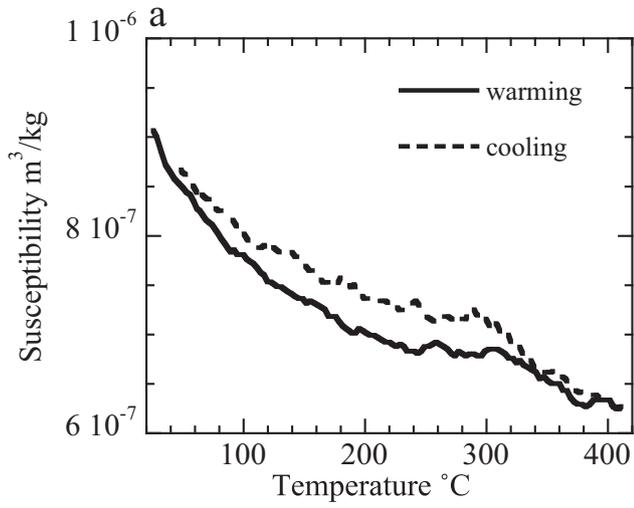
The field cooled and zero-field cooled curves for synthetic Y-98* are identical (Fig. 5e). Both curves show an abrupt loss of remanence below 60 K.

DISCUSSION

Comparison of the magnetic mineral assemblages in the meteorite and the synthetic basalt highlights the importance of iron sulfides and the inadequacy of chromites as recorders of remanence in SNC meteorites. This has implications for assessing the potential for basaltic shergottites to contribute to intense crustal anomalies. Y-980459 magnetic properties are controlled by iron sulfides, which in turn have been affected by shock metamorphism. Shock textures in Y-980459 suggest that this meteorite experienced peak pressures of 20–25 GPa (Greshake et al. 2004). Shock experiments on pyrrhotite indicate that brecciation and formation of microcracks, lattice defects, and planar deformation features are the most common deformation mechanisms at pressures up to 20 GPa (Mang et al. 2013). These features reduce the grain size, produce SD-like regions within larger grains, and broaden and suppress the 34 K transition (Rochette et al. 2003; Louzada et al. 2010; Gilder et al. 2011; Mang et al. 2013), consistent with what we observe in Y-98049. Ni substitution for Fe may also affect the presence and nature of the transition, similar to the effects of cation substitution on the magnetite Verwey transition (Dunlop and Özdemir [1997] and references therein). However, the difference in the FC and ZFC curves of Y-980459 indicates that the shocked pyrrhotite continues to be susceptible to a field-controlled bias in its easy axis of magnetization. We see no twinning or quenched iron metal crystals in Y-980459, features that formed in the 20–30 GPa range during shock pressure experiments (Mang et al. 2013).

The loss of remanence at 55–60 K in both the meteorite and in Y-98* is potentially due to an order/ disorder transition in chromite, for example, a Curie temperature or an isotropic point, or unblocking of a superparamagnetic or paramagnetic phase that is ordered at low temperatures. Previous low-temperature studies of ordinary chondrites interpreted features at 40–80 K as chromite Curie temperatures (Gattacceca et al. 2011). However, Y-98* carries a stable IRM at room temperature and therefore it must contain at least one phase that is ferromagnetic at 300 K. The average composition of chromite in both the natural and the synthetic meteorites has less Fe and Cr than pure $FeCr_2O_4$, which forms a solid solution series with Fe_3O_4. The presence of Mg, Al, and Ti impurities is expected to lower the Curie temperature, reported as 70 K for pure $FeCr_2O_4$ (Robbins et al. 1971; Klemme
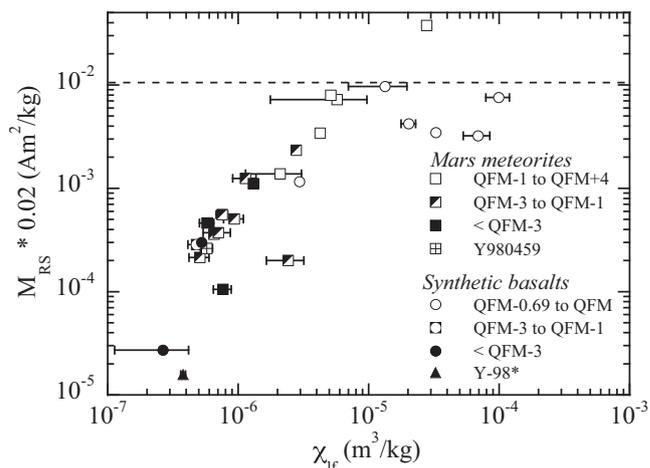

Fig. 6. Saturation magnetization (M_{RS} * 0.02) versus low-field magnetic susceptibility (χ_{lf}) for meteorites of Martian origin, including SNCs and the volcanic breccia NWA 7034, and for synthetic basalts for which fO_2 determinations exist. Standard deviations are shown where available (see Table 4 for data and references). Synthetic basalts synthesized at QFM-0.69 to QFM plot below the main trend. These samples are sulfur-free and have lower $M_{RS}*0.02$ values relative to pyrrhotite-bearing samples. The dashed line at $7*10^{-3}$ Am^2 kg^{-1} (20 A m^{-1} for basalts with a density of 2900 kg m^{-3}) represents the intensity of remanence necessary to generate the observed magnetic anomalies on Mars.

et al. 2000). The 55–60 K feature is likely the Curie temperature for the majority of chromite present. Fe-rich regions or Fe-rich intergrowths may be responsible for carrying the stable IRM acquired at 300 K, although no intergrowths were directly observed. If present, these features are below the imaging resolution of our electron microprobe.

When evaluating the remanence-carrying capabilities of Mars meteorites, Rochette et al. (2005) suggested that the NRM should not be used, as the NRM is likely affected by shock demagnetization that occurred during the ejection event. Instead, they proposed calculating 2% of the M_{RS} value (hereafter denoted $M_{RS}*0.02$) as a proxy for thermoremanent magnetization (TRM). Figure 6 compares $M_{RS}*0.02$ and low-field magnetic susceptibility values for Mars meteorites for which both fO_2 determinations and rock magnetic analyses have been published (Table 4), along with data from iron-rich basalts synthesized at reducing to moderately oxidizing conditions (Brachfeld and Hammer 2006; Bowles et al. 2009). The available data suggest that relatively reduced (<QFM-1) basalts of meteorite character (i.e., Fe-rich and Al-poor), such as Y-980459, are not capable of generating the observed Mars crustal anomalies (Fig. 6). $M_{RS}*0.02$ values in SNC meteorites and synthetic basalts formed at more reducing conditions are 0.5 to 3 orders of magnitude

Table 4. Martian material fO_2 and magnetic parameters.

Name	Type[a]	fO_2 range (ΔQFM)	χ_{lf} (m³ kg⁻¹)	$M_{RS} * 0.02$ (Am² kg⁻¹)	fO_2 ref.	Magnetic ref.
Materials of Martian origin						
NWA 7034/7533	Breccia	>0	2.79E-05	3.76E-02	z	z
MIL 03346	Nakhlite	−0.24 to +0.4	5.13E-06	7.96E-03	k, l	u
Lafayette	Nakhlite	+0.4	2.10E-06	1.38E-03	a, m	s
NWA 998	Nakhlite	−0.8	4.26E-06	3.42E-03	m	u
Los Angeles	Shergottite	−1	5.74E-06	7.20E-03	d, e, i	t
NWA 480/1460	Shergottite	−1.4 to −1.2	2.79E-06	2.34E-03	i	u
Tissint	Shergottite	−1 to −5	1.14E-06	1.25E-03	o, x	x
DaG 476/489/670/1037b	Shergottite	−2.3 to −1.5	7.07E-07	3.72E-04	d, e, f, i, j	t
Yamato 980459	Shergottite	−2.5	5.76E-07	2.80E-04	j	α
Shergotty	Shergottite	−3 to −1	7.57E-07	5.58E-04	c, d, e, i	p, s, t
Zagami	Shergottite	−3 to −2	5.10E-07	2.14E-04	c, d, e, i	p, r, s, t
ALHA77005	Ultramafic	−3 to −2	2.42E-06	2.00E-04	c, h, l	p, q, u
EET A79001A	Shergottite	−3 to −2	6.53E-07	3.60E-04	c, d, e, h	p, q, r, u
EET A79001B	Shergottite	−3 to −2	9.36E-07	5.06E-04	c, d, e	p, q, r, u
Dho 19	Shergottite	−3.8	5.79E-07	4.62E-04	h	t
SaU 005/0990	Shergottite	−3.8	7.66E-07	1.05E-04	g, h, i, j	t, u
QUE 94201	Shergottite	−4.5 to −3	1.31E-06	1.11E-03	b, d, e	u
Gusev crater basalts	–	−3.6 to +0.5	–	–	n	–
Synthetic basalts						
MAm-11 (231 C/h)	M-type	0	1.33E-05	9.68E-03	w	w, y
MAm-13 (72.4 C/h)	M-type	0	2.03E-05	4.22E-03	w	w, y
MAm-12 (18.7 C/h)	M-type	0	3.28E-05	3.46E-03	w	w, y
MAm-20 (5.7 C/h)	M-type	0	6.90E-05	3.22E-03	w	w
MAm-17 (var)	M-type	0	9.94E-05	7.56E-03	w	w
MAm-31 (72.4 C/h)	M-type	−0.69	2.95E-06	1.16E-03	v	v
MAm-19 (231 C/h)	M-type	−1.44	4.82E-07	2.86E-04	v	v
MAm-29 (72.4 C/h)	M-type	−3.44	2.65E-07	2.72E-05	v	v
MA-47 (3 C/h)	A*, Cr-free	−3.44	5.26E-07	3.00E-04	v	v
Y-98*	Y-type	−3.19 to −2.54	3.79E-07	1.58E-05	α	α

[a]M-type basalt has Fe/Al = 1.4 (Bowles et al. 2009). A* is patterned on Chassigny meteorite composition, but lacks Cr and Mn (see Hammer 2006). Y-type is a sulfur-free analog of Yamato 980459, see Table 1, this study.

fO_2 references: a. Bunch and Reid (1975); b. McSween et al. (1996); c. Ghosal et al. (1998); d. Herd et al. (2001); e. Wadhwa (2001); f. Herd et al. (2002); g. Gnos et al. (2002); h. Goodrich et al. (2003); i. Lorand et al. (2005); j. Shearer et al. (2006); k. Righter et al. (2008); l. McCanta et al. (2009); m. Szymanski et al. (2010); n. Schmidt et al. (2013); o. Balta et al. (2015).

Magnetic references: p. Cisowski (1986); q. Collinson (1986); r. Terho et al. (1991); s. Collinson (1997); t. Rochette et al. (2001); u. Rochette et al. (2005); v. Brachfeld and Hammer (2006); w. Bowles et al. (2009); x. Gattacceca et al. (2013); y. Brachfeld et al. (2014); z. Gattacceca et al. (2014); α. This study.

lower than in materials that formed at more oxidizing conditions (QFM-1 to QFM+0.4). Y-980459 (fO_2 = QFM-2.5) plots within a cluster defined by QFM-3 to QFM-1 conditions. The intensity of $M_{RS}*0.02$ in Y-98* is more than an order of magnitude lower than the other natural and synthetic Mars basalts in its fO_2 group. Similarly, ARM and IRM are consistently weaker and less stable in Y-98* (Table 3), highlighting the inadequacy of chromite as a contributor to crustal magnetic anomalies. We note that the precise composition of the spinel is critical, as Fe-Cr-Ti-Mg-Al spinels have been documented as significant carriers of remanence in basaltic shergottite

SaU 008 (Yu and Gee 2005) and in synthetic basalts (Bowles et al. 2009).

The minimum intensity of remanence needed to generate the Mars crustal anomalies is estimated at 20 A m⁻¹ (Nimmo 2000; Brachfeld and Hammer 2006; Bowles et al. 2009), which corresponds to $7*10^{-3}$ Am² kg⁻¹ assuming a basalt density of 2900 kg m⁻³. Only the materials that formed at fO_2 > QFM-1 (comparable to terrestrial redox conditions) approach or exceed this threshold (Fig. 6). This includes the nakhlites, the oxidized Mars breccia NWA 7034 and its paired stones, the oxidized shergottite Tissint, and synthetic basalts generated at

oxidizing conditions (Rochette et al. 2005; Brachfeld and Hammer 2006; Bowles et al. 2009; Gattacceca et al. 2013, 2104). On the basis of Gusev basalt analyses, Schmidt et al. (2013) proposed that the fO_2 range in the Martian mantle is relatively restricted, minimally affected by subduction of oxidized crust, and comparable to conditions that generated basaltic shergottites. While the basaltic and olivine-phyric shergottites are generally more reduced (Table 4), we note this is not the case for all olivine-phyric basalts. For example, Herd (2003) reports an fO_2 value corresponding to QFM+0.2 for the late-crystallizing assemblage in NWA 1110L. This is consistent with the calculation of Righter et al. (2013) that oxidation by up to one fO_2 log unit may occur during decompression of Fe-rich melts from 4 GPa. Such a late-stage oxidation event may not be represented in the phenocryst assemblages of erupted basalts, but could conceivably dominate the magnetic signatures of shallowly emplaced magmas or surface lavas through formation of single-domain titanomagnetite. Furthermore, the presence of liquid water in the upper crust of early Mars could have caused shallowly emplaced magmas to have ferric iron abundances that were different from mantle sources (e.g., Kelley and Cottrell 2009).

Alternately, the Mars crustal magnetic anomalies could result from a combination of primary and secondary processes, for example, primary magmatism and subsequent modification of the igneous crust by crystallization of new minerals within melt sheets immediately after an impact, or later hydrothermal alteration within the crust. Broad spatial correlations have been noted between the locations of strong magnetic anomalies and valley networks (Jakosky and Phillips 2001; Harrison and Grimm 2002; Hood et al. 2010) and between magnetic anomalies, valley networks, and the locations of hydrated minerals (Hood et al. 2010). The presence of liquid water in the upper crust of early Mars could have served as an oxidizing agent during hydrothermal alteration. This interpretation is supported by NWA 7034 and its paired stones. Chemical weathering or hydrothermal alteration likely influenced the highly oxidized NWA 7034, leading to its unique magnetic mineral assemblages (Agee et al. 2013; Gattacceca et al. 2014). The acquisition of a chemical remanent magnetization (CRM) or a thermo-chemical remanent magnetization (TCRM) within a breccia (or within in situ crust) would have depended upon the relative timing of oxide growth and dynamo cessation. It is important to note that the magnetic mineral formation process was likely not the same in NWA 7034 and the SNCs, nor was the remanence acquisition process. If Mars crustal anomalies represent a primary TRM, then oxidizing magmatic conditions were required during basalt cooling. If the Mars crustal anomalies represent a CRM or TCRM, then oxidizing conditions are implied by the character of the breccia class of meteorites.

CONCLUSIONS

A comparison of Martian meteorites and their magnetic properties, which includes new data from a primitive Mg-rich shergottite and its synthetic analog, demonstrates that moderate fO_2 (>QFM-1) is required to generate remanent magnetizations sufficient to produce the crustal anomalies in the Mars Southern Highlands. This is true for both a primary igneous assemblage carrying a TRM, or a secondary assemblage carrying a CRM or TRCM and formed during impact events or hydrothermal alteration. Even "meteorite-type" basalts with high Fe/Al ratios, which have previously been demonstrated to have the greatest potential for acquiring strong remanent magnetizations (Brachfeld and Hammer 2006), produce inefficient magnetic recording assemblages when cooled at low fO_2. Materials such as nakhlites, the oxidized Mars breccia NWA 7034 and its paired stones, the oxidized shergottite Tissint, and synthetic basalts generated at QFM conditions are capable of acquiring remanent magnetizations that approach or exceed 20 A/m (Rochette et al. 2005; Brachfeld and Hammer 2006; Bowles et al. 2009; Gattacceca et al. 2013, 2014). Basalts with low Fe/Al ratios are less capable than the meteorite-based basalts of retaining intense TRM (Bowles et al. 2009). Furthermore, this study demonstrates the need to include sulfur in synthetic analogs to generate basalts that accurately represent the Martian crust. In aggregate, our results suggest that moderately oxidizing conditions were critical on early Mars for generating a mineral assemblage capable of acquiring intense remanent magnetizations, regardless of the remanence acquisition process, basalt character, or thermal history.

REFERENCES

Acuña M. H., Connerney J. E. P., Ness N. F., Lin R. P., Mitchell D., Carlson C. W., McFadden J., Anderson K. A., Rème H., Mazelle C., Vignes D., Wasilewski P., and Cloutier P. 1999. Global distribution of crustal magnetization discovered by the Mars Global Surveyor MAG/ER experiment. *Science* 284:790–793.

Acuña M. H., Connerney J. E. P., Wasilweski P., Lin R. P., Mitchell D., Anderson K. A., Carlson C. W., McFadden J., Rème H., Mazelle C., Vignes D., Bauer S. J., Cloutier P., and Ness N. F. 2001. Magnetic field of Mars: Summary of results from the aerobraking and mapping orbits. *Journal of Geophysical Research* 106:23,403–23,417.

Agee C. B., Wilson N. V., McCubbin F. M., Ziegler K., Polyak V. J., Sharp Z. D., Asmerom Y., Nunn M. H., Shaheen R., Thiemens M. H., Steele A., Fogel M. L., Bowden R., Glamoclija M., Zhang Z., and Elardo S. M. 2013. Unique meteorite from Early Amazonian Mars: Water-rich basaltic breccia Northwest Africa 7034. *Science* 339:780–785.

Armstrong J. T. 1988. Quantitative analysis of silicates and oxide minerals: Comparison of Monte-Carlo, ZAF and Phi-Rho-Z procedures. In *Microbeam analysis*, edited by Newbury D. E. San Francisco, California: San Francisco Press. pp. 239–246.

Balta J. B., Sanborn M. E., Udry A., Wadhwa M., and McSween H. 2015. Petrology and trace element geochemistry of Tissint, the newest shergottite fall. *Meteoritics & Planetary Science* 50:63–85.

Bowles J., Hammer J., and Brachfeld S. 2009. Magnetic and petrologic characterization of synthetic Martian basalts and implications for the surface magnetization of Mars. *Journal of Geophysical Research* 114:E10003.

Boynton W. V., Taylor G. J., Evans L. G., Reedy R. C., Starr R., Janes D. M., Kerry K. E., Drake D. M., Kim K. J., Williams R. M. S., Crombie M. K., Dohm J. M., Metzger A. E., Karunatillake S., Keller J. M., Newsom H. E., Arnold J. R., Brückner J., Englert P. A. J., Gasnault O., Sprague A. L., Mitrofanov I., Squyres S. W., Trombka J. I., d'Uston L., Wänke H., and Hamara D. K. 2007. Concentration of H, Si, Cl, K, Fe, and Th in the low- and mid-latitude regions of Mars. *Journal of Geophysical Research* 112:E12S99.

Brachfeld S. A. and Hammer J. E. 2006. Rock-magnetic and remanence properties of synthetic Fe-rich basalts: Implications for Mars crustal anomalies. *Earth and Planetary Science Letters* 248:599–617.

Brachfeld S., Cuomo D., Tatsumi-Petrochilos L., Bowles J., Hammer J., and Shah D. 2014. Contribution of basaltic intrusions to the intensity and stability of Mars crustal magnetic anomalies. *Geophysical Research Letters* 41:7997–8005.

Bunch T. E. and Reid A. M. 1975. The nakhlites Part I: Petrography and mineral chemistry. *Meteoritics* 10:303–311.

Cisowski S. M. 1986. Magnetic studies on Shergotty and other SNC meteorites. *Geochimica et Cosmochimica Acta* 50:1043–1048.

Collinson D. W. 1986. Magnetic properties of Antarctic shergottite meteorites EETA79001 and ALHA77005: Possible relevance to a Martian magnetic field. *Earth and Planetary Science Letters* 77:159–164.

Collinson D. W. 1997. Magnetic properties of Martian meteorites: Implications for an ancient Martian magnetic field. *Meteoritics & Planetary Science* 32:803–811.

Connerney J. E. P., Acuña M. H., Wasilewski P. J., Ness N. F., Rème H., Mazelle C., Vignes D., Lin R. P., Mitchell D. L., and Cloutier P. A. 1999. Magnetic lineations in the ancient crust of Mars. *Science* 284:749–798.

Day R., Fuller M. D., and Schmidt V. A. 1977. Hysteresis properties of titanomagnetites: Grain size and composition dependence. *Physics of the Earth and Planetary Interiors* 13:260–266.

Dekkers M. J., Mattéi J.-L., Fillion G., and Rochette P. 1989. Grain size dependence of the magnetic behavior of pyrrhotite during its low temperature transition at 34 K. *Geophysical Research Letters* 16:855–858.

Dunlop D. J. and Özdemir Ö. 1997. *Rock magnetism: Fundamentals and frontiers*. Cambridge, UK: Cambridge University Press.

Filiberto J. and Dasgupta R. 2011. Fe^{2+}–Mg partitioning between olivine and basaltic melts: Applications to genesis of olivine-phyric shergottites and conditions of melting in the Martian interior. *Earth and Planetary Science Letters* 304:527–537.

Gattacceca J., Rochette P., Lagroix F., Mathé P.-E., and Zanda B. 2011. Low temperature magnetic transition of chromite in ordinary chondrites. *Geophysical Research Letters* 38:L10203.

Gattacceca J., Hewins R. H., Lorand J.-P., Rochette P., Lagroix F., Cournède C., Uehara M., Pont S., Sautter V., Scorzelli R. B., Hombourger C., Munayco P., Zanda B., Chennaoui H., and Ferrière L. 2013. Opaque minerals, magnetic properties, and paleomagnetism of the Tissint Martian meteorite. *Meteoritics & Planetary Science* 48:1919–1936.

Gattacceca J., Rochette P., Scorzelli R. B., Munayco P., Agee C., Quesnel Y., Cournède C., and Geissman J. 2014. Martian meteorites and Martian magnetic anomalies: A new perspective from NWA 7034. *Geophysical Research Letters* 41:4859–4864.

Ghosal S., Sack R. O., Ghiroso M. S., and Lipschutz M. E. 1998. Evidence for a reduced, Fe-depleted Martian mantle source region of shergottites. *Contributions to Mineralogy Petrology* 130:346–357.

Gilder S. A., Egli R., Hochleitner R., Roud S. C., Volk M. W. R., LeGoff M., and de Wit M. 2011. Anatomy of a pressure-induced, ferromagnetic-to-paramagnetic transition in pyrrhotite: Implications for the formation pressure of diamonds. *Journal of Geophysical Research* 116:B10101.

Gnos E., Hofmann B., Franchi I. A., Al-Kathiri A., Huser M., and Moser L. 2002. Sayh al Uhaymir 094: A new Martian meteorite from the Oman desert. *Meteoritics and Planetary Science* 37:835–854.

Goodrich C. A., Herd C. D. K., and Taylor L. A. 2003. Spinels and oxygen fugacity in olivine-phyric and lherzolitic shergottites. *Meteoritics & Planetary Science* 38:1773–1792.

Greshake A., Fritz J., and Stöffler D. 2004. Petrology and shock metamorphism of the olivine-phyric shergottite Yamato 980459: Evidence for a two-stage cooling and a

single-stage ejection history. *Geochimica et Cosmochimica Acta* 68:2359–2377.

Hammer J. E. 2006. Influence of *f*O$_2$ and cooling rate on the kinetics and energetics of Fe-rich basalt crystallization. *Earth and Planetary Science Letters* 248:618–637.

Harrison K. P. and Grimm R. E. 2002. Controls on Martian hydrothermal systems: Application to valley network and magnetic anomaly formation. *Journal of Geophysical Research* 107:1–1–1–12.

Herd C. D. K. 2003. The oxygen fugacity of olivine-phyric Martian basalts and the components within the mantle and crust of Mars. *Meteoritics & Planetary Science* 38:1793–1805.

Herd C. D. K. 2006. Insights into the redox history of the NWA 1068/1110 Martian basalt from mineral equilibria and vanadium oxybarometry. *American Mineralogist* 91:1616–1627.

Herd C. D. K., Papike J. J., and Brearley A. J. 2001. Oxygen fugacity of Martian basalts from electron microprobe oxygen and TEM-EELS analyses of Fe-Ti oxides. *American Mineralogist* 86:1015–1024.

Herd C. D. K., Borg L. E., Jones J. H., and Papike J. J. 2002. Oxygen fugacity and geochemical variations in the Martian basalts: Implications for Martian basalt petrogenesis and the oxidation state of the upper mantle of Mars. *Geochimica et Cosmochimica Acta* 66:2025–2036.

Hoffman V. H., Funaki M., and Torri M. 2010. Comparing the magnetic signatures of NWA 5789 and Yamato 980459 olivine phyric shergottites (abstract# 5338). 73rd Meeting of Meteoritical Society. New York City, NY. *Meteoritics & Planetary Science* 45:A82.

Hood L. L., Harrison K. P., Langlais B., Lillis R. J., Poulet F., and Williams D. A. 2010. Magnetic anomalies near Apollinaris Patera and the Medusae Fossae Formation in Lucus Planum, Mars. *Icarus* 208:118–131.

Hui H., Peslier A. H., Lapen T. J., Shafer J. T., Brandon A. D., and Irving A. J. 2011. Petrogenesis of basaltic shergottite Northwest Africa 5298: Closed-system crystallization of an oxidized mafic melt. *Meteoritics & Planetary Science* 46:1313–1328.

Humayun M., Nemchin A., Zanda B., Hewins R. H., Grange M., Kennedy A., Lorand J.-P., Göpel C., Fieni C., Pont S., and Deldicque D. 2013. Origin and age of the earliest Martian crust from meteorite NWA 7533. *Nature* 503:513–516.

Jakosky B. M. and Phillips R. J. 2001. Mars' volatile and climate history. *Nature* 412:237–244.

Johnson M. C., Rutherford M. J., and Hess P. C. 1991. Chassigny petrogenesis: Melt compositions, intensive parameters and water contents of Martian (?) magmas. *Geochimica et Cosmochimica Acta* 55:349–366.

Kelley K. and Cottrell E. 2009. Water and the oxidation state of subduction zone magmas. *Science* 325:605–607.

Klemme S., O'Neill H. S. C., Schnelle W., and Gmelin E. 2000. The heat capacity of MgCr$_2$O$_4$, FeCr$_2$O$_4$, and Cr$_2$O$_3$ at low temperatures and derived thermodynamic properties. *American Mineralogist* 85:1686–1693.

Lorand J.-P., Chevrier V., and Sautter V. 2005. Sulfide mineralogy and redox conditions in some shergottites. *Meteoritics & Planetary Science* 40:1257–1272.

Louzada K. L., Stewart S. T., Weiss B. P., Gattacceca J., and Bezaeva N. S. 2010. Shock and static pressure demagnetization of pyrrhotite and implications for the Martian crust. *Earth and Planetary Science Letters* 290:90–101.

Mang C., Kontny A., Fritz J., and Schneider R. 2013. Shock experiments up to 30 GPa and their consequences on microstructures and magnetic properties in pyrrhotite. *Geochemistry Geophysics Geosystems* 14:64–85.

McCanta M. C., Elkins-Tanton L., and Rutherford M. J. 2009. Expanding the application of the Eu-oxybarometer to the lherzolitic shergottites and nakhlites: Implications for the oxidation state heterogeneity of the Martian interior. *Meteoritics & Planetary Science* 44:725–745.

McCoy T. J. and Lofgren G. E. 1999. Crystallization of the Zagami shergottite: An experimental study. *Earth and Planetary Science Letters* 173:397–411.

McSween H. Y., Eisenhour D. D., Taylor L. A., Wadhwa M., and Crozaz G. 1996. QUE 94201 shergottite: Crystallization of a Martian basaltic magma. *Geochimica et Cosmochimica Acat* 60:4563–4569.

McSween H. Y., Taylor G. J., and Wyatt M. B. 2009. Elemental composition of the Martian crust. *Science* 324:736–739.

Misawa K. 2004. The Yamato 980459 shergottite consortium. *Antarctic Meteorite Research* 17:1–12.

Musselwhite D. S., Dalton H. A., Kieffer W. S., and Treiman A. H. 2006. Experimental petrology of the basaltic shergottite Yamato-980459: Implications for the thermal structure of the Martian mantle. *Meteoritics & Planetary Science* 41:1271–1290.

Nimmo F. 2000. Dike intrusion as a possible cause of linear Martian magnetic anomalies. *Geology* 28:391–394.

Nyquist L. E., Bogard D. D., Shih C. Y., Greshake A., Stoffler D., and Eugster O. 2001. Ages and geologic histories of Martian meteorites. *Space Science Reviews* 96:105–164.

Righter K., Yang H., Costin Y., and Downs R. T. 2008. Oxygen fugacity in the Martian mantle controlled by carbon: New constraints from the nakhlite MIL 03346. *Meteoritics & Planetary Science* 43:1709–1723.

Righter K., Danielson L. R., Pando K., Morris R. V., Graff T. G., Agresti D. G., Martin A. M., Sutton S. R., Newville M., and Lanzirotti A. 2013. Redox systematics of Martian magmas with implications for magnetite stability. *American Mineralogist* 98:616–628.

Robbins M., Wertheim G. K., Sherwood R. C., and Buchanan D. N. E. 1971. Magnetic properties and site distributions in the system FeCr$_2$O$_4$-Fe$_3$O$_4$ (Fe2+Cr2-xFex3+O4). *Journal of Physics and Chemistry of Solids* 32:717–729.

Rochette P., Fillion G., Matti J.-L., and Dekkers M. 1990. Magnetic transition at 30-34 Kelvin in pyrrhotite: Insight into a widespread occurrence of this mineral in rocks. *Earth and Planetary Science Letters* 98:319–328.

Rochette P., Lorand J.-P., Fillion G., and Sautter V. 2001. Pyrrhotite and the remanent magnetization of SNC meteorites: A changing perspective of Martian magnetism. *Earth and Planetary Science Letters* 190:1–12.

Rochette P., Fillon G., Ballou R., Brunet F., Ouladdiaf B., and Hood L. 2003. High pressure magnetic transition in pyrrhotite and impact demagnetization on Mars. *Geophysical Research Letters* 30:16.

Rochette P., Gattacceca J., Chevrier V., Hoffmann V., Lorand J.-P., Funaki M., and Hochleitner R. 2005. Matching Martian crustal magnetization and magnetic properties of Martian meteorites. *Meteoritics & Planetary Science* 40:529–540.

Schmidt M. E., Schrader C. M., and McCoy T. J. 2013. The primary fO_2 of basalts examined by the Spirit rover in Gusev Crater, Mars: Evidence for multiple redox states in the Martian interior. *Earth and Planetary Science Letters* 384:198–208.

Shearer C. K., McKay G., Papike J. J., and Karner J. M. 2006. Valence state partitioning of vanadium between olivine-liquid: Estimates of the oxygen fugacity of Y980459 and application to other olivine-phyric Martian basalts. *American Mineralogist* 91:1657–1663.

Shih C.-Y., Nyquist L. E., Wiesmann H., Reese Y., and Misawa K. 2005. Rb-Sr and Sm-Nd dating of olivine-phyric shergottite Yamato-980459: Petrogenesis of depleted shergottites. *Antarctic Meteorite Research* 18:46–65.

Shirai N. and Ebihara M. 2004. Chemical characteristics of a Martian meteorite, Yamato 980459. *Antarctic Meteorite Research* 17:55–67.

Snowball I. F. 1997. The detection of single-domain greigite (Fe_3S_4) using rotational remanent magnetization (RRM) and the effective gyro field (Bg): Mineral magnetic and palaeomagnetic applications. *Geophysical Journal International* 130:704–716.

Szymanski A., Brenker F. E., Palmer H., and El Goresy A. 2010. High oxidation state during formation of Martian nakhlites. *Meteoritics & Planetary Science* 45:21–31.

Terho M., Pesonen L. J., and Kukkonen I. T. 1991. The petrophysical classification of meteorites: New results. Geological Survey of Finland Q29.1/91/1. Espoo, Finland. 95 p.

Thompson G. F. 1990. The anomalous demagnetization of pyrrhotite. *Geophysical Journal International* 103:425–430.

Usui T., McSween H. Y., and Floss C. 2008. Petrogenesis of olivine-phyric shergottite Yamato 980459, revisited. *Geochemica et Cosmochimica Acta* 72:1711–1730.

Wadhwa M. 2001. Redox state of Mars upper mantle and crust from Eu anomalies in shergottite pyroxenes. *Science* 291:1527–1530.

Yu Y. and Gee J. S. 2005. Spinel in Martian meteorite SaU 008: Implications for Martian magnetism. *Earth and Planetary Science Letters* 232:287–294.